

Chungpyo Hong¹

Department of Mechanical Engineering,
Kagoshima University,
1-21-40 Korimoto,
Kagoshima 890-0065, Japan
e-mail: hong@mech.kagoshima-u.ac.jp

Yutaka Asako

Fellow ASME
Department of Mechanical Precision
Engineering,
Malaysia-Japan International Institute of
Technology,
University Technology Malaysia,
Jalan Sultan Yahya Petra,
Kuala Lumpur 54100, Malaysia

Mohammad Faghri

Fellow ASME
Department of Mechanical, Industrial and
Systems Engineering,
University of Rhode Island,
2 East Alumni Avenue,
Kingston, RI 02881

Ichiro Ueno

Department of Mechanical Engineering,
Faculty of Science and Technology,
Tokyo University of Science,
2641 Yamazaki,
Noda, Chiba 278-8510, Japan

Heat Transfer of Turbulent Gaseous Flow in Microtubes With Constant Wall Temperature

In this paper, we report on experimental results to measure the total temperature of nitrogen gas at the inlet and outlet of microtubes with constant wall temperature and to quantitatively determine the heat transfer rates. Experiments were conducted with nitrogen gas flowing in a stainless steel microtube with a diameter of 524 μm and a copper microtube with a diameter of 537 μm . The temperature differences between the inlet and the wall were maintained at 3, 5, and 10 K by circulating water around the inlet and the wall. The stagnation pressures were also controlled so that the flow, with atmospheric back pressure, could reach Reynolds numbers as high as 26,000. To measure the total temperature, a polystyrene tube with a thermally insulated exterior wall containing six plastic baffles was attached to the outlet. Heat transfer rates were obtained from the gas enthalpy difference by using the pressures and the total temperatures measured at the inlet and outlet. Heat transfer rates were also compared with those obtained from the ideal gas enthalpy using the measured total temperatures and from the Nusselt number of incompressible flows. It was found that the measured total temperature at the microtube outlet was higher than the wall temperature. Also, the heat transfer rates calculated from the total temperature difference were higher than the values obtained from the incompressible flow theory. [DOI: 10.1115/1.4053215]

Keywords: convection heat transfer, total enthalpy, total temperature, gas flow, microtube

1 Introduction

The need for understanding heat transfer in microgeometries, particularly for applications in micro-electromechanical systems, has been of great interest in recent literature. Wu and Little [1] published results on the first experimental work on heat transfer in microgas flows by measuring friction coefficients and Nusselt numbers for nitrogen, argon, and helium gas flows in silica and glass microchannels. Their results laid the groundwork for the creation of extensive literature with a focus on the heat transfer characteristics of gaseous flows in microchannels. Using nitrogen flow in microtubes with inner diameters ranging from 3 to 81 μm , Choi et al. [2] obtained lower values of the Nusselt number compared with those obtained using empirical correlations. Yu et al. [3] studied fluid flow and heat transfer characteristics of nitrogen gas and water flows in circular tubes with diameters of 15, 52, and 102 μm . Their Nusselt number values were not in agreement with the correlations given by Wu and Little [1] and Choi et al. [2]. Hara et al. [4] experimentally investigated heat transfer rates of air flow in square mini channels with hydraulic diameters ranging from 0.3 to 2 mm and channel lengths ranging from 10 to 100 mm. The values of the Nusselt number were higher or lower than the Dittus–Boelter correlation depending on the hydraulic diameter and the tube length. To obtain heat transfer rate or the Nusselt number for gaseous flow through microtubes, it is necessary to precisely measure gas temperature at the inlet and outlet.

Morini [5] reported on the importance of accurate gas temperature measurements for low gas flow in microtube, which was

strongly nonuniform in both, the axial and the radial, directions due to the gas stratification.

Yang et al. [6] experimentally investigated forced convection heat transfer characteristics of air in stainless-steel microtubes with inside diameters of 86, 308, and 920 μm , where the tube walls were heated by Joule's effect. They used liquid crystal thermography and thermocouples to measure the surface temperature of the microtubes. They also reported that the conventional heat transfer correlations for laminar and turbulent flows could be applied in the prediction of fully developed gaseous flow and heat transfer performance in microtubes. Yang et al. [7], experimentally and numerically, investigated the characteristics of nitrogen gas convective heat transfer in commercial stainless-steel microtubes with inner diameters of 170, 510, and 750 μm . The specific correlations proposed for the prediction of the Nusselt number failed in the presence of strong compressibility.

Recently, Mohseni et al. [8] analytically investigated the effect of wall slip on the convective heat transfer of gaseous flow in micro-annulus. Dai et al. [9] simulated the argon gas flow in the transition regime and the effect of rarefaction in the heat transfer in microchannels confined between isothermal and nonisothermal parallel plates.

A total temperature probe is widely used for temperature measurements of high-speed gas flows in conventionally sized tubes [10]. Hong et al. [11–13] and Isobe et al. [14] measured the total temperature for gas flow in microtubes with a constant wall temperature. They reported that the measured total temperature was higher than the wall temperature due to the additional heat transfer from the wall. However, the exact position of the total temperature probe was not specified. For this reason, Hong et al. [15] measured the total temperature at locations 2–3.5 mm from the microtube outlet, and the outlet total temperature was then extrapolated from the total temperatures measured at these positions.

¹Corresponding author.

Contributed by the Heat Transfer Division of ASME for publication in the JOURNAL OF HEAT TRANSFER. Manuscript received July 20, 2021; final manuscript received December 1, 2021; published online January 18, 2022. Assoc. Editor: Brian D. Iverson.

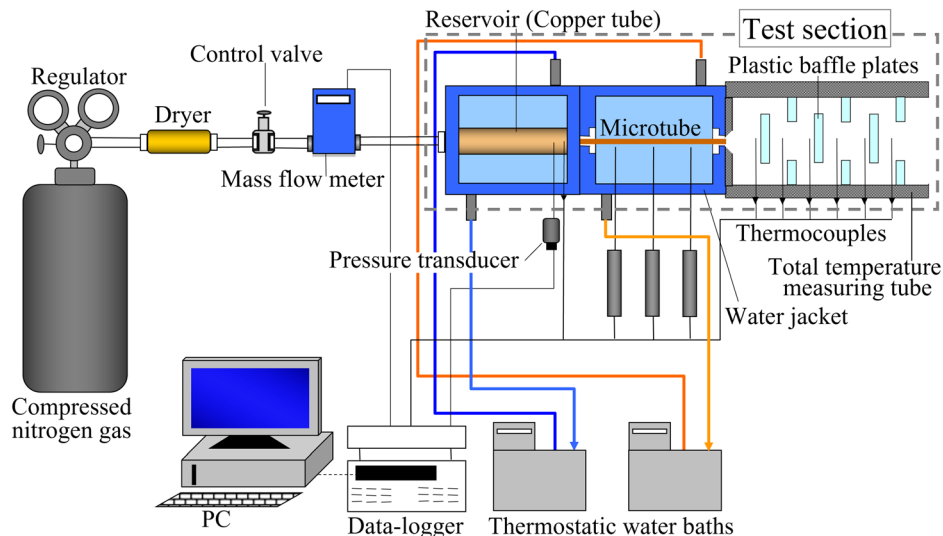


Fig. 1 Schematic view of the experimental setup

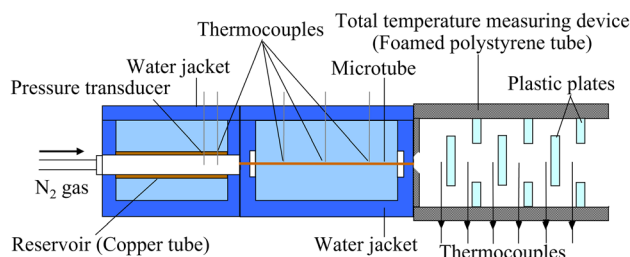


Fig. 2 Detail view of the test section

Yamada et al. [16] pointed out other complications in the temperature measurement using thermocouples in high-speed gas flow. The thermocouple indicated a higher temperature than the static temperature but lower than the total temperature due to the heat transfer from its surface to microjet. Therefore, to measure the total temperature, an externally adiabatic foamed polystyrene tube with six plastic baffles was used. As can be seen from the literature search earlier, the total temperature measurement at the microtube outlet was well investigated in the previous studies [11–15]. However, there seems to be no previous experimental investigation for obtaining heat transfer rates for gaseous flow in microtubes which is the focus of this study.

2 Experimental Setup

The schematic view of the experimental setup is shown in Fig. 1. As shown in this figure, nitrogen from the gas cylinder passes through the regulator, gas dryer, mass flowmeter (Kofloc, Kyoto, Japan, 3100, 10L/min or 30L/min), and the test section. Then, it goes through the microtube and into the temperature measuring device. The schematic view of the heat transfer test section is shown in Fig. 2. It consists of an inlet copper tube, a microtube, and a total temperature measuring device. The inlet copper tube is placed inside a water jacket to control the gas

temperature. The inner diameter, outer diameter, and the length of the inlet copper tube were 6 mm, 8 mm, and 70 mm. A thermocouple was inserted at the center in the radial direction at 60 mm from the inlet to measure the stagnation temperature of the gas. To obtain the temperature difference between the measured temperature and the bulk temperature at the outlet, $T_{c,res} - T_{b,res}$, a supplemental numerical computation was performed for all the experimental runs ($Re_{res} = 300 \sim 1500$) based on the semi-implicit method for pressure-linked equations (SIMPLE) algorithm of Patankar [17]. It was assumed that the velocity, pressure, temperature, and density profiles were uniform at the inlet. Using the numerical calculations, the normalized bulk temperature and center temperature were obtained and tabulated in Table 1 (column (a) and (b)). The normalized temperature difference between the bulk and center temperatures (column (c)) was then obtained from these temperatures. The temperature difference between the wall and the center temperatures, $T_{w,res} - T_{c,res}$ (column (d)), was obtained from $T_{w,res} - T_{c,res} = (T_{w,res} - T_{in,res}) - (T_{c,res} - T_{in,res})$. This measured temperature difference was less than 0.2 K. Substituting 0.2 K for $T_{w,res} - T_{c,res}$, the temperature difference between the wall and the inlet, $T_{w,res} - T_{in,res}$, was calculated, and it ranged from 0.200 K to 0.304 K. The temperature difference between the bulk and the center ranged from 0.10 K to 0.06 K. Therefore, the temperature was assumed to be uniform in the cross section of the inlet copper tube. The thermocouple and the pressure transducer were inserted at the copper tube inlet to measure the gas stagnation pressure (p_{stg}) and stagnation temperature (T_{stg}).

In this study, a stainless steel microtube with a diameter of $524 \mu\text{m}$ and a copper microtube with a diameter of $537 \mu\text{m}$ were used. The details of the measurement were documented in our previous paper [18]. The representative uncertainties were as follows: tube length L , $\pm 10 \mu\text{m}$; water temperature, $\pm 0.2 \text{ K}$; weight, $\pm 10 \text{ mg}$; time, $\pm 0.1 \text{ s}$. From these values, the uncertainty of the tube diameter was estimated as $\pm 0.21\%$. The cross-sectional view of the microtube is depicted in Fig. 3 using a microscope, and the dimensions are listed in Table 2.

Table 1 Bulk, center and wall temperatures in the reservoir

Re	(a)	(b)	(c)	(d)	(e)
	$\frac{T_{b,res} - T_{in,res}}{T_{w,res} - T_{in,res}}$	$\frac{T_{c,res} - T_{in,res}}{T_{w,res} - T_{in,res}}$	$\frac{T_{b,res} - T_{c,res}}{T_{w,res} - T_{in,res}}$	$\frac{T_{w,res} - T_{c,res}}{T_{w,res} - T_{in,res}}$	$T_{b,res} - T_{c,res} \text{ (K)}$
300	0.674	0.343	0.331	0.657	0.10
1500	0.319	0.002	0.317	0.998	0.06

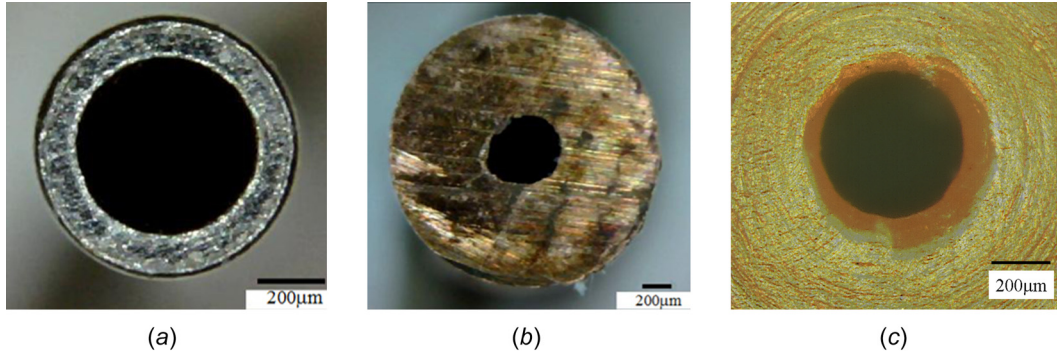


Fig. 3 Microscope pictures of the microtube cross section (a) stainless steel, (b) copper, and (c) PEEK

Table 2 Microtube dimensions

Microtube	Inner diameter, D (μm)	Outer diameter (μm)	Thickness (μm)	Length (mm)	Thermal conductivity (W/(m·K))
Stainless steel (SUS304)	524	810	143	100	16
Copper (C1220)	537	2000	731.5	100	398

The wall temperature was estimated by equating the heat transfer rate by natural convection from the outer wall of the microtube to the heat transfer rate by forced convection through the microtube as follows:

$$\dot{m}(h_{T,\text{out}} - h_{\text{stg}}) = h_m \pi D_o L (T_\infty - T_w) \quad (1)$$

where T_w is the wall temperature and T_∞ is the water temperature in the water jacket. Also, h_m is the mean heat transfer coefficient by natural convection and is determined by the mean-Nusselt number correlation below for the cylinder [19]

$$\text{Nu}_{d,m} \left(= \frac{h_m D_o}{\lambda} \right) = C_2 \left[0.669 \left(\frac{\text{Pr}}{\text{Pr} + \sqrt{\text{Pr} + 0.5}} \right)^{1/4} (\text{PrGr}_d)^{1/4} \right] \quad (2)$$

where C_2 is 0.773 for a cylinder, Gr_d is the Grashof number, and Pr is the Prandtl number.

Then, the temperature difference between the water temperature, T_∞ , and the tube outer wall temperature, T_w , was estimated by Eq. (2) for all cases, with $T_w - T_{\text{stg}} = 3 \text{ K}$, 5 K , and 10 K for both the stainless steel and the copper microtubes. They were tabulated in Table 3. The estimated temperature difference, $T_\infty - T_w$, was less than 0.01 K . Therefore, the value of the water temperature in the water jacket was used for the wall temperature in the data reduction. The microtube was placed inside the lower water jacket to make the wall temperature constant and water circulated between the water jacket and the thermally controlled water bath. The water temperature in the water jacket was measured by three thermocouples of the sheathed type-K with a diameter of 0.5 mm . They were placed 5 mm from the inlet, at the center of the water jacket, and 5 mm from the outlet, and 1 mm away from the microtube outer wall.

A pressure transducer was attached to the upstream chamber to measure the inlet stagnation pressure of the microtube. The

Table 3 $T_\infty - T_w$ for all cases

$T_w - T_{\text{stg}}$	Stainless steel tube	Copper tube
3 K	0.002 ~ 0.008 K	0.002 ~ 0.004 K
5 K	0.002 ~ 0.01 K	0.001 ~ 0.006
10 K	0.004 ~ 0.016 K	0.003 ~ 0.01

temperatures of the gas near the inlet and the outlet of the microtube were measured as shown in Fig. 2. The gas temperature at the inlet was measured by a bare-wire type-K thermocouple, $50 \mu\text{m}$ in diameter, and an adiabatic foamed polystyrene tube with six plastic baffle plates was attached to the microtube outlet to measure the total temperature [16]. The foamed polystyrene tube with an inner diameter of 22 mm was thermally insulated from the surroundings. As can be seen from Fig. 4, two different plastic baffle plates of the ring and rectangular type spaced at the intervals of 5 and 10 mm were used to investigate the effect of plate locations on the reduction of the gas velocity. The gas total temperatures were measured by six bare wire type-T thermocouples, $300 \mu\text{m}$ in diameter, at the baffle plates. More detailed description of the total temperature measurement was documented in a previous paper [16]. Finally, the thermocouples, the pressure transducers, and the flowmeter were connected to the data acquisition system (Eto Denki, Tokyo, Japan, CADAC21) and all the data were simultaneously collected, and the values were averaged.

The uncertainties of the measured values including the temperatures measured by the thermocouples are listed in Table 4 using the methodology by Kee et al. [20]. The values of the overall uncertainty, u_{Overall} , in the table were obtained by using the root-sum-of-squares of the individual uncertainties. This included the uncertainty of the resolution limit of temperature indication, $u_{\text{resolution}}$, the uncertainty due to the resolution limit of voltage measurement, u_{voltage} , the uncertainty of the reference junction compensation, u_{RJC} , and the uncertainty of fluctuation, $u_{\text{fluctuation}}$. The temperature differences, $T_{\text{rj}} - T_{\text{internal}}$, of the input channels nos. 3 to 17 used for the temperature measurements are plotted in

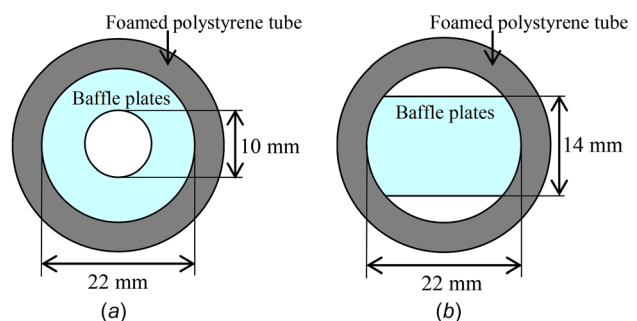


Fig. 4 Baffles in temperature measuring device (a) ring type and (b) rectangular type

Table 4 Uncertainties of experimental measurements

Measurements	Uncertainties				
<i>Pressure</i>					
Valcom VESX (0 ~ 500 kPa)	±0.25 % of F.S. (±1.25 kPa)				
<i>Flow rate</i>					
KOFLOC 3100 (0 ~ 10,000 cc/min)	±1.00 % of F.S. (±100 cc/min)				
<i>Temperature</i>					
	$u_{\text{Overall}} = \sqrt{u_{\text{resolution}}^2 + u_{\text{voltage}}^2 + u_{\text{RJC}}^2 + u_{\text{fluctuation}}^2}$				
Thermocouple (Type-T and K)	u_{Overall} (°C)	$u_{\text{resolution}}$ (°C)	u_{voltage} (°C)	u_{RJC} (°C)	$u_{\text{fluctuation}}$ (°C)
	±0.116	±0.0289	±0.0518	±0.1	±0.0058

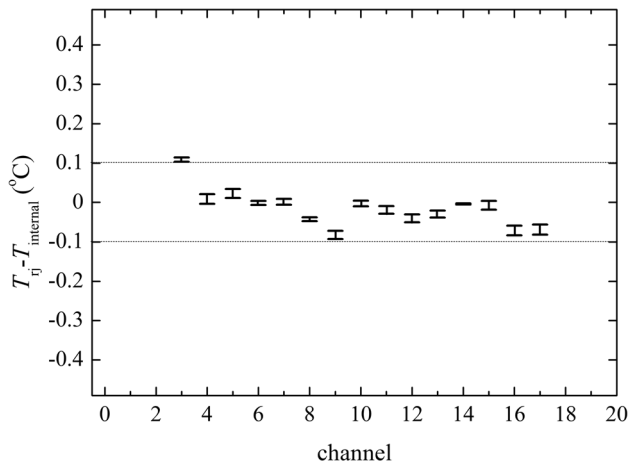


Fig. 5 Temperature difference between reference junction and internal temperatures

Fig. 5. T_{rj} is the temperature of the reference junction (temperature of the terminal) and T_{internal} is the temperature that is used for the reference junction compensation. $T_{rj} - T_{\text{internal}}$ expresses the reference junction compensation error that is affected by the environment and its uncertainty is $\pm 0.1^\circ\text{C}$ which is relatively small. The overall uncertainty of the measured temperature by the thermocouple was $\pm 0.116^\circ\text{C}$.

In this study, the repeatability of the temperature measurements was also obtained. The six bare wire type-T thermocouples, 300 μm in diameter, were used to measure the gas total temperatures at the six baffle plates. The stagnation air temperature in the adiabatic box was measured 4 times per minute in an interval of 1 s with one of the six thermocouples and resistance temperature detector (RTD). Each measurement was conducted about 30 min after the data acquisition system was powered to reach steady-state. The histogram of the temperature difference between the thermocouple and RTD, $T_{T\text{-type}} - T_{\text{RTD}}$, for one of the four measurements is plotted in Fig. 6. The values of $T_{T\text{-type}} - T_{\text{RTD}}$ were 0 K or 0.1 K since the resolution of the thermocouple and RTD for the data acquisition system was 0.1 K and 0.01 K, respectively. The average and the standard deviation of $T_{T\text{-type}} - T_{\text{RTD}}$ are tabulated in Table 5 to show the repeatability of the temperature measurements.

3 Validation of Total Temperature Measurement

The heat transfer rates from the microtube wall to the flowing gas were obtained from the total enthalpy difference between the microtube inlet and outlet using the methodology suggested by Yamada et al. [16]. A polyether ether ketone (PEEK) tube with a nominal inner diameter and outer diameter of 500 μm and 1.6 mm,

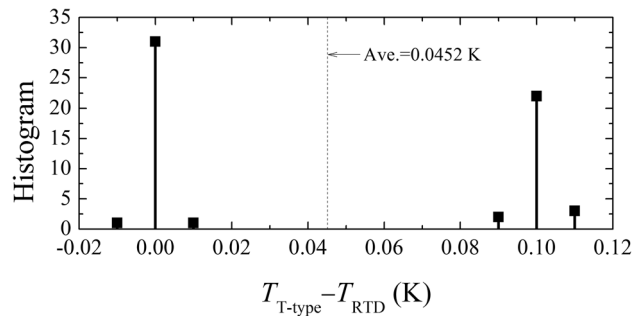


Fig. 6 Histogram of $T_{T\text{-type}} - T_{\text{RTD}}$

Table 5 Average and standard deviation of the values of $T_{T\text{-type}} - T_{\text{RTD}}$

Time	Number	Average of $T_{T\text{-type}} - T_{\text{RTD}}$	Standard deviation of $T_{T\text{-type}} - T_{\text{RTD}}$
1	60	0.0452	0.0505
2	60	0.0333	0.0484
3	60	0.0058	0.0347
4	60	0.0312	0.0399

was used for estimating the total temperature. The cross-sectional view of this tube is depicted in Fig. 3(c) using a microscope. The measured total temperatures at the baffle plates, $T_{T, \text{baffle}}$, with baffle plate spacing of 5 mm are plotted in Fig. 7(a) as a function of the distance from the microtube outlet, x_{exit} . The measured stagnation temperature is also plotted in this figure with dotted lines.

The total enthalpy, $h_{T, \text{baffle}}$ was obtained from the measured total temperature and the atmospheric pressure since the pressure at the baffle plate p_{baffle} is atmospheric pressure. The total enthalpies are plotted in Fig. 7(b) as a function of the distance from the microtube outlet, x_{exit} . The stagnation enthalpy obtained from the measured stagnation temperature and pressure is also plotted in this figure with dotted lines. The measured temperatures at the first baffle plate at $x_{\text{exit}} = 5 \text{ mm}$ were lower than the temperatures at the other locations when the stagnation pressure increased. In an ideal situation, the temperature on the surface of the thermocouple junction placed inside the high-speed gas flow indicates the total temperature if we assume there is no heat transfer from the surface of the thermocouple junction to the flow. This is because the gas velocity approaches zero at the surface. However, there is heat transfer to the flow from the surface of the thermocouple junction. Therefore, the temperature measured is neither the local static temperature nor the total temperature. This temperature is higher than the static temperature but lower than the total temperature [21]. As a result, the total enthalpies at the

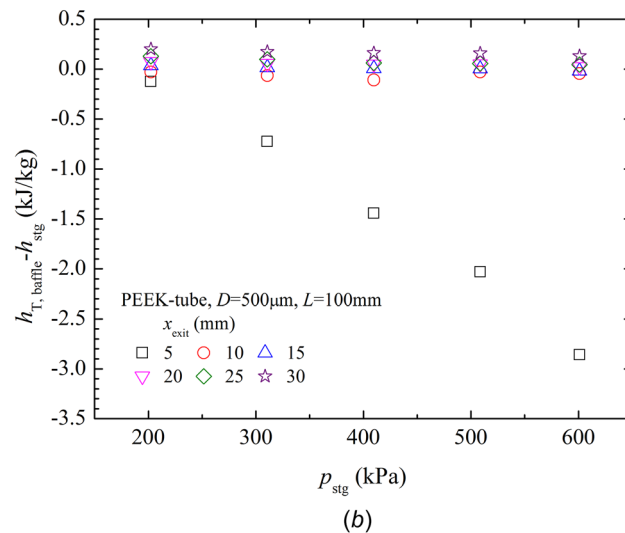
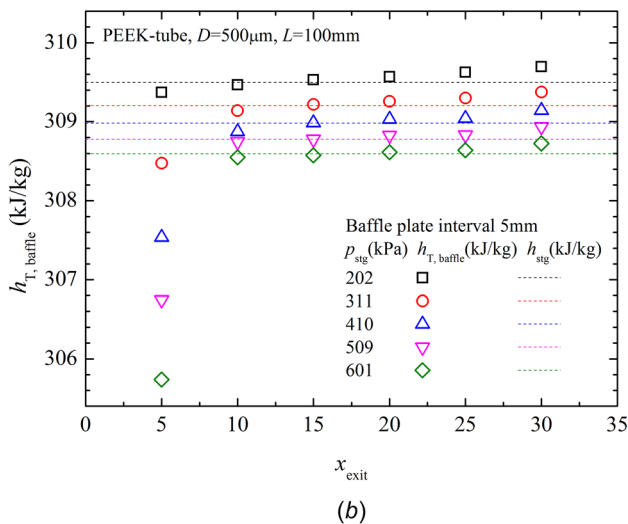
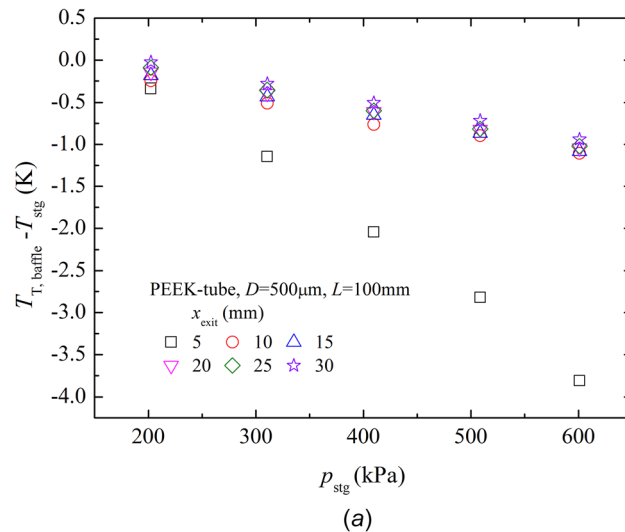
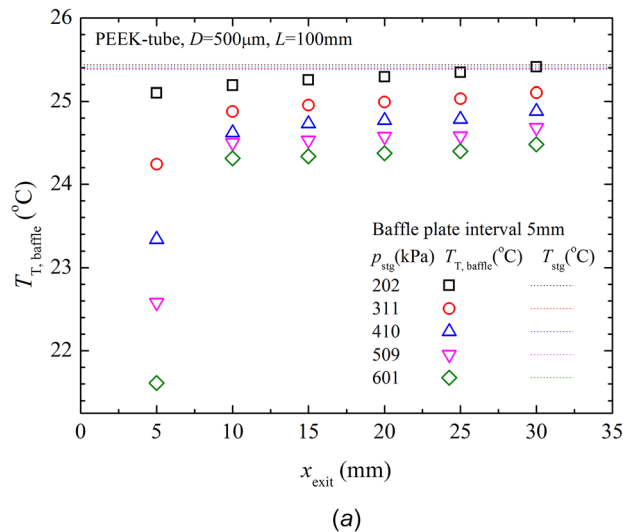


Fig. 7 Total temperature and total enthalpy as a function of x_{exit} (a) total temperature and (b) total enthalpy

first baffle plate were lower than the enthalpies at the other locations. The total temperatures at the second baffle plate and consecutive locations coincided with the averaged values to within $\pm 0.13^\circ\text{C}$.

The total temperature difference between the baffle plate and the stagnation, $T_{T, \text{baffle}} - T_{\text{stg}}$ is plotted in Fig. 8(a) as a function of the stagnation pressure. The total enthalpy difference between the baffle plate and the stagnation, $h_{T, \text{baffle}} - h_{\text{stg}}$ is also plotted in Fig. 8(b) as a function of the stagnation pressure. As the stagnation pressure increased, $T_{T, \text{baffle}} - T_{\text{stg}}$ decreased but the corresponding total enthalpy difference was nearly zero because the microtube and the total temperature measuring device were externally insulated. For the case of no shaft work and no heat input from the tube wall to the gas, the first law of thermodynamics for the case of steady flow can be expressed as (e.g., Ref. [22])

$$h_{\text{stg}} = h_{\text{in}} + \frac{u_{\text{in}}^2}{2} = h_{\text{out}} + \frac{u_{\text{out}}^2}{2} = h_{T, \text{out}} \quad (3)$$

As mentioned in Sec. 2, an externally adiabatic foamed polystyrene tube with six plastic baffle plates was attached to the microtube outlet that was thermally insulated from the surroundings. Therefore, the flow can be assumed to be isenthalpic and if there is no heat input from the wall to the gas, then

$$h_{T, \text{out}} = h_{T, \text{baffle}} \quad (4)$$

Fig. 8 Total temperature difference and total enthalpy difference as a function of p_{stg} (a) total temperature difference and (b) total enthalpy difference

As can be seen in Fig. 8(b), the stagnation enthalpy coincides with the total enthalpy at the baffle plates. Therefore, there is no heat loss or gain in the total temperature measuring tube.

If the gas expands in an isenthalpic manner, the gas temperature increases or decreases depending on the Joule–Thomson coefficient. The Joule–Thomson coefficient of nitrogen gas under atmospheric temperature and pressure takes a value of $\mu_{J, T} = 2.2$ (K/MPa) [23]. This means that the gas temperature decreases by 2.2 K when the pressure difference is 1 MPa. Therefore, $T_{T, \text{baffle}} - T_{\text{stg}}$ decreased with an increase in the stagnation pressure in Fig. 8(a). Note that the pressure at the microtube outlet increased when the flow at the outlet was choked. The pressure at the microtube outlet is required to obtain the temperature but since it is hard to be measured, the total enthalpy at the outlet was obtained from the total enthalpy at the baffle plate using Eq. (4).

4 Results and Discussion

The present experiments were carried out using a stainless steel microtube and a copper microtube. The temperature of the water bath was adjusted such that the temperature difference between the wall and the stagnation temperature was varied in the range of 3 K to 10 K. After setting the temperature, tests were carried out for various flow conditions. The stagnation pressure ranged from 200 to 600 kPa in 50 or 100 kPa intervals. The experimental

Table 6 Experimental results of $T_{\text{stg}} \approx 294$ K and $T_w \approx 297$ K for stainless microtube

p_{stg} (kPa)	\dot{m} (kg/s)	Re	Ma_{in}	T_{stg} (K)	T_w (K)	$T_{T, \text{baffle, ave}}$ (K)
150	2.610×10^{-5}	3629	0.206	293.5	296.6	297.0
203	4.167×10^{-5}	5807	0.246	293.7	296.7	297.5
251	5.457×10^{-5}	7610	0.262	293.8	297.1	298.1
300	6.732×10^{-5}	9382	0.271	294.2	297.3	298.4
353	8.072×10^{-5}	11249	0.277	294.2	297.3	298.5
406	9.382×10^{-5}	13069	0.280	294.3	297.3	298.5
454	1.059×10^{-4}	14755	0.283	294.4	297.3	298.4
507	1.186×10^{-4}	16517	0.284	294.4	297.3	298.3
556	1.309×10^{-4}	18219	0.286	294.5	297.3	298.3
604	1.431×10^{-4}	19905	0.288	294.5	297.2	298.2

results for the cases of $T_{\text{stg}} \approx 294$ K and $T_w \approx 297$ K for the stainless microtube are tabulated in Table 6.

4.1 Total Enthalpy. The temperatures measured at the baffle plates are almost the same except for the temperature at $x_{\text{exit}} = 5$ mm as shown in Fig. 7(a). Therefore, the average temperatures at the second to the sixth baffle plates, $T_{T, \text{baffle, ave}}$ were assumed to be the total temperature. The total temperature, total enthalpy, the inlet Mach number, and mass flow rate are plotted as a function of p_{stg} in Fig. 9 with $T_{\text{wall}} - T_{\text{stg}}$ shown as a dotted line. The total enthalpy at the microtube outlet, $h_{T, \text{out}}$ is equal to $h_{T, \text{baffle}}$, if there is no heat transfer between the microtube outlet and the sixth baffle plate. The Ma_{in} is

$$Ma_{\text{in}} = \frac{u_{\text{in}}}{a_{\text{in}}} \quad (5)$$

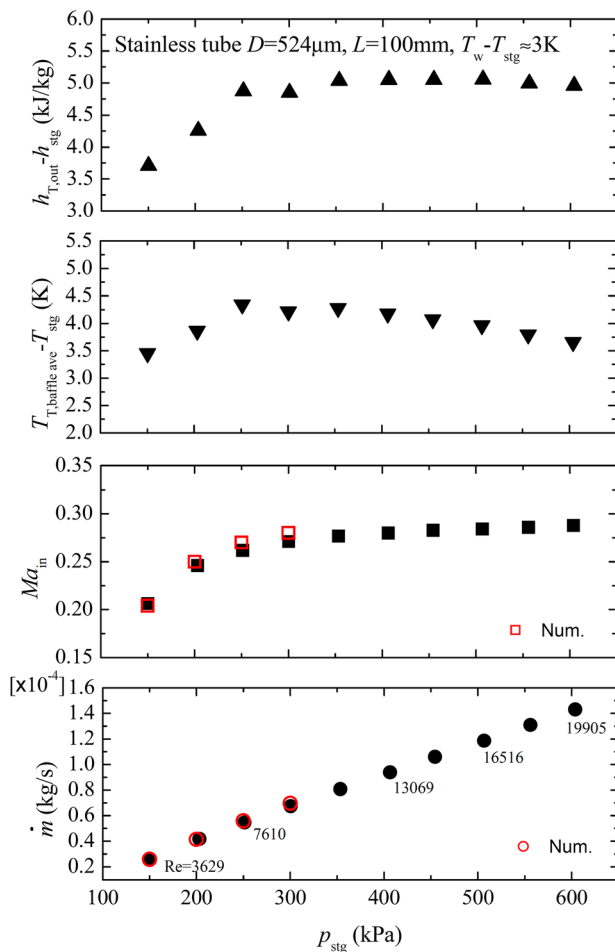


Fig. 9 Total temperature, total enthalpy, inlet Mach number and mass flow rate as a function of p_{stg}

where a_{in} is the speed of sound at the inlet, which is obtained by using the density and static enthalpy at the inlet as

$$a_{\text{in}} = a(\rho_{\text{in}}, h_{\text{in}}) \quad (6)$$

The values of velocity, density, and static enthalpy at the inlet can be obtained under the assumptions of isentropic and real gas conditions as follows:

$$u_{\text{in}} = \frac{\dot{m}}{\rho_{\text{in}} A}, \quad \rho_{\text{in}} = \rho(h_{\text{in}}, h_{\text{stg}}), \quad h_{\text{in}} = h_{\text{stg}} - \frac{u_{\text{in}}^2}{2} \quad (7)$$

where, $S_{\text{stg}} = S(p_{\text{stg}}, T_{\text{stg}}) = S_{\text{in}}$ and A is the cross-sectional area of the microtube.

The values of velocity, density, and static enthalpy at the inlet are extrapolated by solving Eq. (5). The results for the stainless microtube for $T_{\text{stg}} \approx 294$ K and $T_w \approx 297$ K are shown in Fig. 9. To validate the accuracy of the experimental data, supplemental numerical computations were performed based on the arbitrary-Lagrangian-Eulerian method for the same experimental conditions of the unchoked flow ($p_{\text{stg}} = 150 \sim 300$ kPa in Table 6). The detailed description of the numerical methodology is documented in the previous work [24]. As can be seen in this figure, the experimental and numerical results are in excellent agreement.

The total temperature in Fig. 9 is higher than the wall temperature because it includes the kinetic energy component of the gas on top of the stagnant temperature. The same results were reported in previous studies [11,12,25]. The inlet Mach number increased with an increase in the stagnation pressure, and nearly leveled off for $p_{\text{stg}} \geq 300$ kPa when the flow was choked. $T_{T, \text{baffle, ave}} - T_{\text{stg}}$ increased with an increase in the stagnation pressure and slightly decreased for $p_{\text{stg}} \geq 300$ kPa due to gas expansion. However, $h_{T, \text{out}} - h_{\text{stg}}$ increased with an increase in the stagnation pressure and attained its maximum value for $p_{\text{stg}} \geq 300$ kPa. Note that the value of $h_{T, \text{out}} - h_{\text{stg}}$ remained nearly constant when the flow was choked even though the stagnation pressure was increased. The $h_{T, \text{out}} - h_{\text{stg}}$ of the microtube is proportional to the heat transfer rate from the wall. Therefore, the heat transfer rate is a function of mass flow rate when the flow is choked.

Attention is now turned to the bulk and total temperature of the gas [26]. The local bulk temperature averaged over the cross section is defined by

$$T_b = \frac{\int \rho c_p r u T dr}{\int \rho c_p r u dr} \quad (8)$$

and the total temperature is defined by

$$T_T = \frac{\int \rho c_p r u T dr + \int \rho r u (u^2/2) T dr}{\int \rho c_p r u dr} \quad (9)$$

The second term on the right side in Eq. (9) is the kinetic temperature.

The outlet total temperature can be obtained from the outlet total enthalpy if the gas is assumed to be ideal as

$$T_{T, \text{out}} = h_{T, \text{out}} / c_p \quad (10)$$

The total temperatures at the microtube outlet obtained from Eq. (10) are plotted in Fig. 10. The following correlation was obtained by the exponential curve fit:

$$T_{T, \text{out}} - T_{\text{stg}} = 5.05 - 12.02 e^{-p_{\text{stg}}/69.24} \quad (11)$$

For the case of adiabatic wall and real gas, the total temperature decreases at the outlet and is proportional to the Joule Thomson

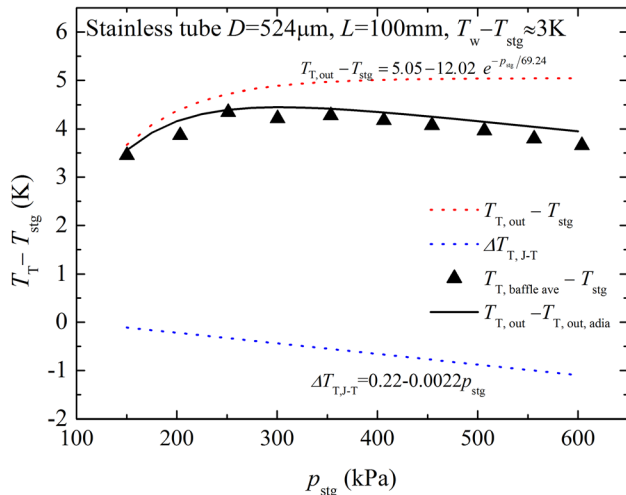


Fig. 10 Total temperature as a function of p_{stg}

coefficient. The total temperatures at the outlet are plotted in Fig. 10 for nitrogen. The following correlation is obtained by a linear curve fit:

$$\Delta T_{T,J-T} = 0.22 - 0.0022 p_{stg} \quad (12)$$

where $\Delta T_{T,J-T}$ is the change in temperature.

In the above equation, the temperature decreases because of the gas expansion due to the pressure difference between the inlet and the outlet (Joule Thomson effect). Equations (11) and (12) are plotted in Fig. 10 as a function of the stagnation pressure with the red and blue dotted lines, respectively. The sum of the Eqs. (11) and (12), $(T_{T,out} - T_{stg}) + \Delta T_{T,J-T}$ and the values of $T_{T,baffle\ ave} - T_{stg}$ in Fig. 9 are also plotted in this figure with solid and triangular lines, respectively, and both are in excellent agreement. When the flow is not choked ($p_{stg} < 300$ kPa), heat was transferred from the wall to the gas, and the increase in temperature was more significant than the decrease in temperature by the gas expansion. As a result, the total temperature at the microtube outlet increased for $p_{stg} < 300$ kPa as shown in this figure. However, when the flow was choked ($p_{stg} \geq 300$ kPa), heat was transferred from the wall to the gas, because the velocities and the static temperatures inside the microtubes were limited.

4.2 Heat Transfer Rate. The heat transfer rate is obtained by

$$\dot{Q}_h = \dot{m} (h_{T,out} - h_{stg}) \quad (13)$$

For an ideal gas, the enthalpy is a function of temperature as

$$dh = c_{p,ave} dT \quad (14)$$

And the heat transfer rate is

$$\dot{Q}_T = \dot{m} c_p (T_{T,baffle\ ave} - T_{stg}) \quad (15)$$

In the case of low flow velocities for an ideal gas, the heat transfer rate can be expressed using the bulk temperature at the outlet since $T_T \approx T_b$

$$\dot{Q}_{slow} = \dot{m} c_p (T_{b,incomp} - T_{in}) \quad (16)$$

where $T_{b,incomp}$ is the bulk temperature for an incompressible flow and is obtained by the mean Nusselt number (e.g., Burmeister [27])

$$T_{b,incomp} = T_w - (T_w - T_{stg}) e^{-4Nu_m X^*} \quad (17)$$

For the case of a turbulent fully developed flow in ducts, the mean Nusselt number was obtained by [28]

$$Nu_m = 0.022 Re^{0.8} Pr^{0.5} \quad (18)$$

where X^* in Eq. (17) is the inverse of Graetz number, defined by

$$X^* = \frac{x}{D Re Pr} \quad (19)$$

The heat transfer rates were obtained by Eqs. (13), (15), and (16) by using the measured data. The heat transfer rate normalized by \dot{Q}_{slow} , \dot{Q}_h/\dot{Q}_{slow} , and \dot{Q}_T/\dot{Q}_{slow} is plotted as a function of the stagnation pressure in Fig. 11. $T_{T,out}$ in Eq. (15) has the same value as $T_{T,baffle\ ave}$ at the baffle plate in the total temperature measuring device because the flow is isenthalpic. Therefore, \dot{Q}_T was obtained by substituting $T_{T,baffle\ ave}$ into $T_{T,out}$. Part of the thermal energy converts into kinetic energy near the outlet at high flow velocities. This results in a decrease in the bulk temperature, and an additional heat transfer from the wall to the gas. Therefore, both values of \dot{Q}_h/\dot{Q}_{slow} and \dot{Q}_T/\dot{Q}_{slow} were greater than one. In the case of $T_w - T_{stg} = 10$ K, the maximum discrepancy for both values due to additional heat transfer was less than 20%. However, in the cases of $T_w - T_{stg} = 3$ K and $T_w - T_{stg} = 5$ K, the maximum discrepancy was more than 80% and 40%, respectively. The value of \dot{Q}_T/\dot{Q}_{slow} increased, as p_{stg} increased and leveled off for the choked flow ($p_{stg} \geq 300$ kPa). In this case, the measured $T_{T,baffle\ ave}$ slightly decreased with an increase in the p_{stg} as shown in Fig. 9. Therefore, \dot{Q}_T/\dot{Q}_{slow} calculated using the temperature difference, $T_{T,out} - T_{stg}$, remained nearly constant as p_{stg} increased. However, the value of \dot{Q}_h/\dot{Q}_{slow} increased with an increase in the p_{stg} since $\frac{T_{c,res} - T_{in,res}}{T_{w,res} - T_{in,res}}$ was calculated by the enthalpy difference, $h_{T,out} - h_{stg}$. Therefore, the values of \dot{Q}_h/\dot{Q}_{slow} were higher than \dot{Q}_T/\dot{Q}_{slow} . The values of $\frac{T_{b,res} - T_{c,res}}{T_{w,res} - T_{in,res}}$ are plotted in Fig. 12 as a function of the stagnation pressure. It decreased with an increase in the stagnation pressure, and for the smaller temperature difference between T_w and T_{stg} . In the case of $T_w - T_{stg} = 3$ K, its maximum value decreased by more than 25%. Therefore, the heat transfer rate was calculated by the enthalpy difference using the temperature and pressure.

Both the thicknesses and thermal conductivities of the copper and stainless steel microtubes are listed in Table 2. Their inner diameters in Table 2 are nearly the same even though their

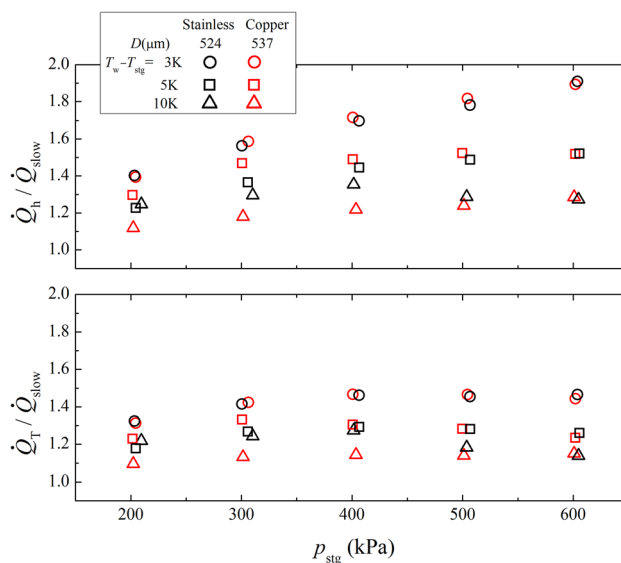


Fig. 11 Heat transfer rates as a function of p_{stg}

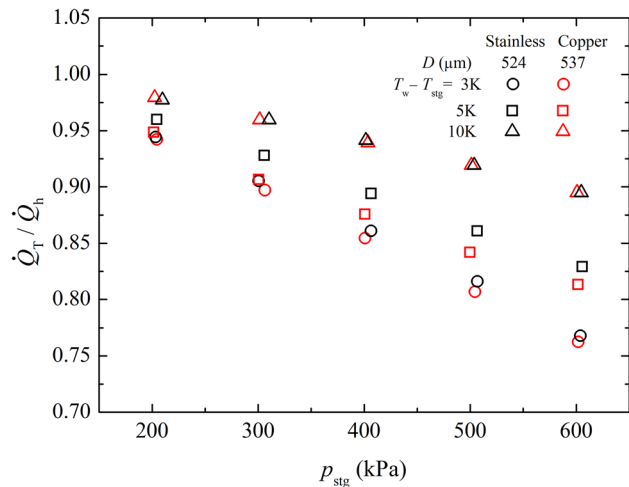


Fig. 12 Heat transfer rates as a function of p_{stg}

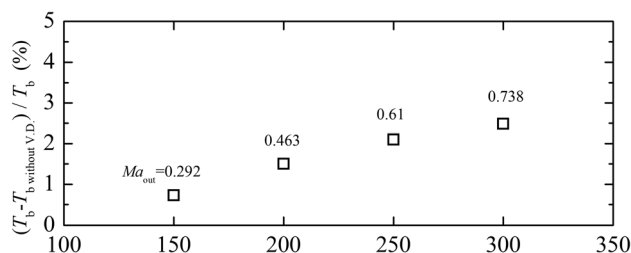


Fig. 13 Difference between T_b and T_b without v.d. as a function of p_{stg}

thicknesses and thermal conductivities are different. The wall temperature is constant along the tube for the present thermal boundary condition of constant wall temperature since the copper microtube has high thermal conductivity and is thick. It was found that the wall temperature of the stainless steel microtube was constant along the tube even though the conductivity of the stainless steel microtube was lower than that of the copper microtube.

4.3 Effects of Viscous Dissipation and Slip (Rarefaction) on the Wall. Supplemental numerical computations were performed with or without viscous dissipation term in the energy equation for the unchoked flow cases of $T_{stg} = 294$ K and $T_w = 297$ K. The bulk temperature and the Mach number were obtained at the tube outlet. The difference between T_b and T_b without v.d. is plotted in Fig. 13 as a function of p_{stg} with the Mach number as a parameter. It increased with an increase in the Mach number, but its value was relatively small. Note that the bulk temperature of compressible flow was very close to the temperature obtained without both viscous dissipation and compressibility terms although the Mach number at the outlet reached 0.7.

The rarefaction effect by slip velocity, temperature jump, and shear work on the wall depends on the Knudsen number that is the ratio of the gas mean path to the tube diameter. It is dominant for the tube diameters less than $10 \mu\text{m}$, and it is negligible for this study where the tube diameters are $524 \mu\text{m}$ and $537 \mu\text{m}$ and the Knudsen number is 1.3×10^{-4} under atmospheric pressure and room temperature for the tube diameter of $524 \mu\text{m}$.

5 Conclusions

In this study, the total temperature at the inlet and outlet were measured to determine the heat transfer rates of nitrogen gas flow in stainless steel and copper microtubes with diameters of 524 and

$537 \mu\text{m}$ and constant wall temperatures. The conclusions are summarized as follows:

- (1) The gas bulk temperature decreased because of thermal energy conversion to kinetic energy and therefore the measured total temperature at the outlet was higher than the wall temperature.
- (2) The values of $T_{T, \text{baffle ave}} - T_{stg}$ increased with the increase in p_{stg} and slightly decreased in the range when the flow was choked. However, the values of $h_{T, \text{out}} - h_{stg}$ increased with the increase in the p_{stg} and attained its maximum value. $\frac{T_{w, \text{res}} - T_{c, \text{res}}}{T_{s, \text{res}} - T_{sp, \text{res}}}$ calculated from the total enthalpy difference and \dot{Q}_T calculated from the total temperature difference were higher than \dot{Q}_{slow} obtained from the incompressible flow theory, and the difference between \dot{Q}_h and \dot{Q}_T was large when the flow was choked because of the Joule-Thomson effect.
- (3) The same heat transfer rates were obtained for the copper microtube with high thermal conductivity and the stainless steel microtube with low thermal conductivity.

Nomenclature

- a = speed of sound (m/s)
- A = cross-sectional area (m^2)
- c_p = specific heat at constant pressure ($\text{J}/(\text{kg K})$)
- D = tube diameter (m)
- Gr = Grashof number
- h = heat transfer coefficient ($\text{W}/(\text{m}^2 \text{K})$)
- h = specific enthalpy (J/kg)
- L = length (m)
- \dot{m} = mass flow rate (kg/s)
- Ma = Mach number
- Nu = Nusselt number
- p = pressure (Pa)
- Pr = Prandtl number
- \dot{Q} = heat transfer rate (W)
- Re = Reynolds number
- s = specific entropy ($\text{J}/(\text{kg K})$)
- T = temperature (K)
- u = velocity (m/s)
- u = uncertainty
- x = axial distance from microtube entrance (m)
- X^* = inverse of Graetz number
- $\mu_{J.T.}$ = Joule-Thomson coefficient (K/MPa)
- ρ = density (kg/m^3)

Subscripts

- ave = averaged value
- b = bulk
- baffle = baffle plate
- c = center
- d = cylindrical tube
- fluc = fluctuating value
- h = specific enthalpy
- in = microtube inlet
- incomp = incompressible value
- inst = instrument value
- internal = internal value for reference junction compensation
- J-T = Joule Thomson effect
- m = mean value
- o = outside
- out = microtube outlet
- Overall = overall value
- res = reservoir
- sj = reference junction
- RJC = reference junction compensation
- RTD = resistance temperature detector

slow = slow flow
 stg = stagnation value
 T = total temperature
 T-type = T-type thermocouple
 w = wall
 ∞ = surrounding properties

References

- [1] Wu, P. Y., and Little, W. A., 1984, "Measurement of the Heat Transfer Characteristics of Gas Flow in Fine Channel Heat Exchangers Used for Microminature Refrigerators," *Cryogenics*, **24**(8), pp. 415–420.
- [2] Choi, S. B., Barron, R. F., and Warrington, R. O., 1991, "Fluid Flow and Heat Transfer in Micro Tubes," *Micro Mechanical Sensors, Actuators and Systems*, ASME, New York, Paper No. DSC-32, pp. 123–134.
- [3] Yu, D., Warrington, R., Barron, R., and Ameel, T., 1995, "An Experimental and Theoretical Investigation of Fluid Flow and Heat Transfer in Microtubes," *ASME/JSME Thermal Engineering Conference Vol.1*, pp. 523–530.
- [4] Hara, K., Inoue, M., and Furukawa, M., 2007, "Heat Transfer in Mini-Channel Gaseous Cooling," *J. Environ. Eng.*, **2**(3), pp. 525–534.
- [5] Morini, G. L., 2012, "The Rule of Single-Phase Forced Convection in Microchannels," *ASME Paper No. ICNMM2012-73253*.
- [6] Yang, C., Chen, C., Lin, T., and Kandlikar, S. G., 2012, "Heat Transfer and Friction Characteristics of Air Flow in Microtube," *Exp. Therm. Fluid Sci.*, **37**, pp. 12–18.
- [7] Yang, Y., Hong, C., Morini, G. L., and Asako, Y., 2014, "Experimental and Numerical Investigation of Forced Convection of Subsonic Gas Flows in Microtubes," *Int. J. Heat Mass Transfer*, **78**, pp. 732–740.
- [8] Mohseni, M. M., Tissot, G., and Badawi, M., 2020, "Effects of Wall Slip on Convective Heat Transfers of Gaseous Fluid in Microannulus," *ASME J. Heat Transfer-Trans. ASME*, **142**(8), p. 082503.
- [9] Dai, L., Wu, H., and Tang, J., 2020, "The UGKS Simulation of Microchannel Gas Flow and Heat Transfer Confined Between Isothermal and Nonisothermal Parallel Plates," *ASME J. Heat Transfer-Trans. ASME*, **142**(22), p. 122501.
- [10] Yahya, S. M., 2006, *Fundamentals of Compressible Flow With Aircraft and Rocket Propulsion*, 3rd ed., New Age International Publishers, New Delhi, India.
- [11] Hong, C., Yamamoto, T., Asako, Y., and Suzuki, K., 2012, "Heat Transfer Characteristics of Compressible Laminar Flow Through Microtubes," *ASME J. Heat Transfer-Trans. ASME*, **134**(11), p. 011602.
- [12] Hong, C., Asako, Y., Ueno, I., and Motosuke, H., 2014, "Total Temperature Measurement of Laminar Gas Flow at Microtube Outlet: Cooled From the Wall," *Heat Transfer Eng.*, **35**(2), pp. 142–149.
- [13] Hong, C., Uchida, Y., Yamamoto, T., Asako, Y., and Suzuki, K., 2010, "Heat Transfer Characteristics of Turbulent Gas Flow Through Micro-Tubes," *ASME Paper No. IHTC14-22355*.
- [14] Isobe, K., Hong, C., Asako, Y., and Ueno, I., 2011, "Heat Transfer Characteristics of Gas Flow in Micro-Tubes With Constant Wall Temperature," *Proceedings of the 4th International Conference on Heat Transfer and Fluid Flow in Microscale*, Fukuoka, Japan, Paper No. Hiffm-IV-068.
- [15] Hong, C., Isobe, K., Asako, Y., and Ueno, I., 2013, "Total Temperature Measurement of Turbulent Gas Flow at Microtube Exit," *ASME Paper No. ICNMM2013-73180*.
- [16] Yamada, M., Hong, C., and Asako, Y., 2014, "Total Temperature Measurement of Micro-Gas Jet," *ASME Paper No. IMECE2014-36965*.
- [17] Patankar, S. V., 1980, *Numerical Heat Transfer and Fluid Flow*, Hemisphere Publishing Corporation, New York.
- [18] Asako, Y., Nakayama, K., and Shinozuka, T., 2005, "Effect of Compressibility on Gaseous Flows in a Micro-Tube," *Int. J. Heat Mass Transfer*, **48**(23–24), pp. 4985–4994.
- [19] Hermann, R., 1954, "Heat Transfer by Free Convection From Horizontal Cylinders in Diatomic Gases," NASA, Washington, DC, Report No. NACA-TM-1366.
- [20] Kee, Y. Y., Asako, Y., Ken, T. L., and Sidik, N. A. C., 2020, "Uncertainty of Temperature Measured by Thermocouple," *J. Adv. Res. Fluid Mech. Therm. Sci.*, **68**(1), pp. 54–62.
- [21] Kulkarni, K. S., Madanan, U., and Goldstein, R. J., 2020, "Effect of Freestream Turbulence on Recovery Factor of a Thermocouple Probe and Its Consequences," *Int. J. Heat Mass Transfer*, **152**, p. 119498.
- [22] Cengel, Y. A., and Boles, M. A., 1989, *Thermodynamics: An Engineering Approach*, McGraw-Hill.
- [23] NIST, 2013, "NIST Reference Fluid Thermodynamic and Transport Properties-REFPROP 9.1," Gaithersburg, MD.
- [24] Isobe, K., Hong, C., Asako, Y., and Ueno, I., 2011, "Numerical Simulation on Heat Transfer Characteristics of Turbulent Gas Flow in Micro-Tubes," *ASME Paper No. IMECE2011-64513*.
- [25] Hong, C., and Asako, Y., 2014, "Convective Heat Transfer of Unchoked and Choked Gas Flow in Micro-Tubes," *ASME Paper No. ICNMM2014-21740*.
- [26] Hong, C., and Asako, Y., 2007, "Heat Transfer Characteristics of Gaseous Flows in Microchannels and Microtubes With Constant Wall Temperature," *Numer. Heat Transfer Part A*, **52**(3), pp. 219–239.
- [27] Burmeister, L. C., 1983, *Convection Heat Transfer*, 2nd ed., Wiley, Singapore.
- [28] Kays, W. M., and Crawford, M. E., 1980, *Convection Heat and Mass Transfer*, 2nd ed., McGraw-Hill, New York.